The effect of inhomogeneities on the infrared reststrahlen band of beryllium oxide

1995 J. Phys.: Condens. Matter 7 8507

(http://iopscience.iop.org/0953-8984/7/45/006)

J. Phys.: Condens. Matter 7 (1995) 8507–8518. Printed in the UK

The effect of inhomogeneities on the infrared reststrahlen band of beryllium oxide

Stefan K Andersson and Gunnar A Niklasson

Solid State Physics, Department of Technology, Box 534, Uppsala University, S-751 21 Uppsala, *Sweden*

Received 31 July 1995

Abstract. We have measured the infrared–optical properties of ceramic beryllium oxide and observed a pronounced reflectance minimum in the reststrahlen band. This feature can be due to phonon absorption in voids in the material or in surface bumps and pits. Calculated reflectance spectra for each of these mechanisms show qualitative agreement with experiment and both effects are probably present in our experimental situation. A small reflectance dip corresponding to the longitudinal optical phonon mode was observed in our experiments. For a bulk sample, this mode can only be excited by bumps at the surface. This shows that phonon absorption in surface features is of great importance for the reststrahlen band in beryllium oxide.

1. Introduction

The infrared–optical properties of ionic or partly ionic materials are dominated by the so-called reststrahlen band between the transverse optical (TO) and the longitudinal optical (LO) phonon frequencies, ω_T and ω_L. Transverse electromagnetic waves can interact with transverse optical phonons and the quantum of the coupled field is called a polariton. In the reststrahlen region the real part of the dielectric function is negative, which leads to a high reflectance from the surface of a slab of the material. In addition the material is strongly absorbing, and the imaginary part of the dielectric function exhibits a resonance at the transverse optical phonon frequency.

In the case of small crystallites of ionic material, the position of the polariton resonance depends on their size and shape [1]. The situation is particularly simple for particles that are much smaller than the wavelength of the incident electromagnetic field. In the case of spheres, Fröhlich [2] showed that the resonance peak occurs at a frequency, ω_F, between the TO and LO ones. This is also the case for ellipsoids [3] but here one peak is obtained for each of the three depolarization factors that describe the shape of the ellipsoid. In a similar way voids in an ionic material give rise to resonances in the reststrahlen band.

Roughness in the form of protrusions from and pits in the surface also modifies the features in the reststrahlen band significantly. These effects were first observed by Barker [4] who discovered so-called forbidden optical modes, sensitive to surface treatment, in sapphire. Berreman [5] modelled the surface roughness with hemispherical bumps and pits. He showed that structure appears in the reststrahlen band, because of the excitation of resonances associated with the surface inhomogeneities. In the case of surface features much smaller than the wavelength, quasistatic theories for a variety of shapes now exist. This is mainly due to the efforts of the Leiden group, who have treated the optical properties

0953-8984/95/458507+12$19.50

of truncated spheres [6, 7] and spheroids [8] on a substrate. Their theory was used in our recent study [9] of the optical phonon absorption of surface inhomogeneities.

In this work we study features of the reststrahlen band for beryllia, but the effects are general for all ionic or partly ionic materials. Recent studies of beryllia [10] have shown the existence of a minimum in the reststrahlen band, characteristic of polycrystalline material, in contrast to early results for a single crystal [11]. It was later shown [12] that the reflectance minimum could be understood from a simple model of phonon absorption in inhomogeneities at the surface. The surface roughness was represented by free ellipsoidal spheroids with different shapes and directions. In the present work we carry out a more detailed analysis of the minimum in the reststrahlen band.

The purpose of the present paper is twofold. We introduce a more realistic model of the surface roughness, representing it with truncated spherical bumps and pits. In our quasistatic calculation we take into account the multipolar interactions with the substrate and the dipole–dipole interactions with the other particles and their images in the substrate. The model cannot treat high coverages of truncated spheres on a surface, but qualitative comparisons with experiments can be carried out. We also study the effects of pores in the bulk of the ceramic beryllia on the infrared properties. For this purpose we used the Bruggeman [13] effective-medium approximation (EMA) to determine the average dielectric function of the porous material. The aim is to distinguish between effects of surface features and pores.

A clear indication of the importance of surface roughness for the infrared properties was obtained in the observation of a LO resonance for p-polarized light incident at an oblique angle. It is well known that the LO mode can be excited in a thin film [14, 16] of an ionic material, but it is usually not possible in a bulk material. We have shown [9] that an absorption peak in the LO mode position arises when the surface is covered by small truncated spherical bumps.

In section 2 below we describe sample preparation and the experimental techniques. In subsection 3.1 we briefly describe the effective-medium model and in section 3.2 the truncated sphere or so-called bump model of the surface features is presented. The comparison between the experimental and calculated results is discussed in section 4, followed by some concluding remarks in section 5.

2. Samples and experimental methods

The specular normal reflectance of beryllium oxide was measured with a FT-IR Bomen–Michelson 110 spectrometer. For measurements where the samples were coated with paraffin oil, the spectrometer was equipped with a Labsphere 4/5 in. Infragold integrating sphere and a cooled mercury cadmium telluride detector. Measurements at oblique angles of incidence were carried out with a Perkin–Elmer 157 infrared spectrometer.

The polycrystalline beryllium oxide samples, with grain sizes in the range 10–20 μm were prepared on a large scale by green forming a powder slurry and subsequently firing the shaped part. The material is specified to have 99.5% purity. The density was measured as 2.90 g cm^{-3} as compared to 3.01 g cm^{-3} for a single crystal. The beryllia sample was 0.6 mm thick.

The surface of the polycrystalline beryllia sample was analysed with a JEOL scanning electron microscope (SEM). To avoid charging the highly insulating surface, the sample had to be covered with a thin layer of gold. This gold layer was deposited by sputtering and its thickness was 2 nm. The surface was also analysed with an atomic force microscope (AFM), Nanoscope III, contact mode. The surface structure of the samples is shown in figure 1.

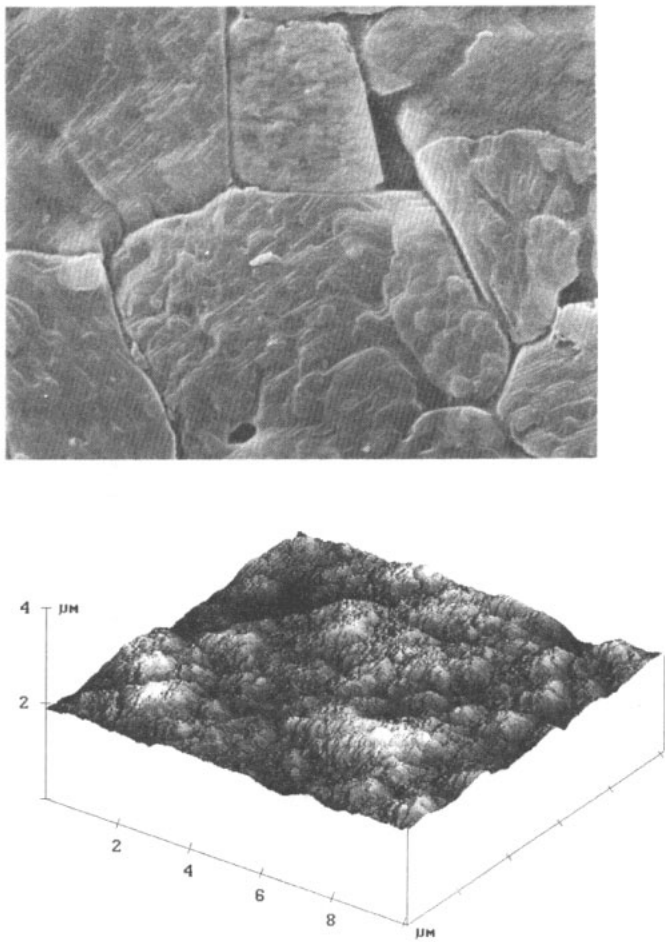

Figure 1. The upper panel shows a scanning electron microscope image of the ceramic BeO surface coated with a thin gold film. The lower panel shows an AFM picture of one crystal of the polycrystalline beryllia surface.

The upper panel of figure 1 shows voids and grain boundaries between the crystallites and that each crystallite exhibits pronounced surface features. In the AFM picture in the lower panel of figure 1 the topography of part of a crystallite is shown. The surface protrusions or bumps may vary in both size and shape. The root mean square (RMS) roughness of a crystallite was found to be 74 nm and the maximum peak to valley distance was 674 nm. Both parameters increase with measurement area because the voids associated with grain boundaries will influence the result more and more. For example, a 125 × 125 μm area exhibited a RMS roughness of 178 nm and a peak-to-valley value of 2.01 μm.

The optical properties of polycrystalline beryllia were derived from a fit of the classical oscillator dispersion formula to the reflectance spectra. The expression for the complex dielectric function is [3]

$$\varepsilon(\omega) = \varepsilon_\infty + \frac{\omega_T^2(\varepsilon_0 - \varepsilon_\infty)}{\omega_T^2 - \omega^2 + \mathrm{i}\Gamma\omega} \tag{1}$$

where ε_∞ and ε_0 are the high-frequency and static dielectric constants, respectively, and Γ

is the phenomenological damping term. In order to obtain the dielectric function of pure polycrystalline BeO, we neglected the reststrahlen band structure due to inhomogeneities. The transverse and longitudinal optical phonon frequencies were easily obtained from fits to the edges of the reststrahlen band. Subsequently the ratio $\varepsilon_\infty/\varepsilon_0$ was obtained from the Lyddane–Sachs–Teller relation [17]. The optical properties of crystalline beryllia have been studied very little. Loh [11] has evaluated the ordinary and extraordinary infrared complex refractive indices of single crystals from polarized reflectance spectra. To describe polycrystalline samples we use $\varepsilon_\infty = 2.95$ and $\Gamma = 12.0\ \text{cm}^{-1}$, which is consistent with Loh's data. Fits to experimental spectra then gave $\omega_T = 709\ \text{cm}^{-1}$ and $\varepsilon_0 = 7.01$.

3. Theory

3.1. Porous ceramics

Bohren and Gilra [18] showed that voids in the bulk of an ionic material give rise to absorption peaks. In order to take this effect into account we calculate the average dielectric function for the porous material.

Consider an inhomogeneous material consisting of two materials p (particle) and m (matrix). An effective-medium approximation, EMA, describes the optical properties of the mixture in terms of an effective dielectric function $\langle\varepsilon\rangle$ which depends on the dielectric functions of the constituents and their respective volume fractions. Pecharromán and Iglesias [19] used the Bruggeman model [13] for spheroids to determine the effective dielectric function from

$$\left(\frac{2(1-f)(\langle\varepsilon\rangle-\varepsilon_m)}{(1-L_m)\langle\varepsilon\rangle+L_m\varepsilon_m}+\frac{(1-f)(\langle\varepsilon\rangle-\varepsilon_m)}{2L_m\langle\varepsilon\rangle+(1-2L_m)\varepsilon_m}\right)+\left(\frac{2f(\langle\varepsilon\rangle-\varepsilon_p)}{(1-L_p)\langle\varepsilon\rangle+L_p\varepsilon_p}+\frac{f(\langle\varepsilon\rangle-\varepsilon_p)}{2L_p\langle\varepsilon\rangle+(1-2L_p)\varepsilon_p}\right)=0 \tag{2}$$

where f, the filling factor, is the volume fraction of 'p' material and ε_p and ε_m are the dielectric functions of the particle and the matrix respectively. The triplet of depolarization factors for the p and m materials are given by $(L_p,\ L_p,\ 1-2L_p)$ and $(L_m,\ L_m,\ 1-2L_m)$, respectively. For our samples BeO is considered to be the 'm' material and air is the 'p' material.

In order to obtain the reflectance we consider the light to be incident onto a homogeneous layer characterized by $\langle\varepsilon\rangle$. The reflectances for s- and p-polarized light were calculated by the well-known Fresnel formulae [20].

3.2. Bump model

In this section we briefly describe the bump model for the reflectance from a rough surface. The approximation is based on the general theory of Vlieger *et al* [6–8] for the optical properties of truncated spheres on a substrate. The surface roughness is modelled by truncated spheres and holes, bumps and pits, much smaller than the wavelength. In this quasistatic limit, the electrical potential is obtained from a solution of the Laplace equation.

Consider a truncated sphere on a substrate, as depicted in figure 2. We introduce a truncation parameter $r_0 = d/R$, where d is the distance from the substrate to the centre of the sphere and R is the radius of the sphere. The centre is, in our model, always situated below the surface of the substrate which yields that $r_0 \leqslant 0$. A homogeneous electric field (E) is incident from the ambient medium (1). The Laplace equation has to be solved in the

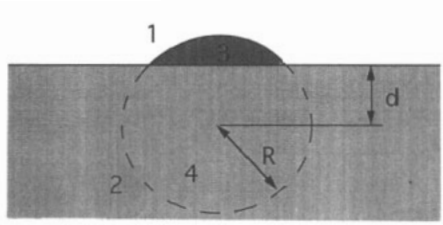

Figure 2. Cross section of a truncated sphere on a substrate. The numbers 1–4 illustrate the regions where the Laplace equation has to be solved.

ambient, in the substrate (2), in the truncated sphere (3) and in the region (4) in the substrate. Berreman [5] first solved this problem for the case of hemispheres and subsequently the problem was solved for a general truncated sphere by Bobbert, Wind, Bedeaux and Vlieger [6, 8] in terms of an expansion in multipoles and image multipoles.

It is possible to use the same theory to carry out calculations for pits and holes in the substrate. This is accomplished by dividing all the dielectric functions in the geometry of figure 2, with the dielectric function of the substrate, ε_s. The electric field is now incident from the region (2).

In the case of touching particles or particles touching a substrate, the convergence of the multipole expansion is a very difficult issue. Haarmans and Bedeaux [21] have investigated the convergence for the case of metal spheres on a transparent substrate. For low coverages they find that 15 to 19 multipoles are necessary to obtain accuracy of 10^{-5}. In our calculation we use 16 multipoles, in order to take into account the interaction between the particle and the substrate. We think that this should be a good approximation to the exact result.

From the electrical potential one easily obtains the polarizability, α [6,9]. This quantity depends on the direction of the incident electric field relative to the surface. The polarizabilities for the E-field parallel and perpendicular to the surface are denoted $\alpha_\parallel$ and $\alpha_\perp$, respectively.

The interaction between different particles must also be considered. By far the most important contribution comes from dipole–dipole interactions [7]. Only the dipole–dipole term is therefore taken into account in our calculations and higher-order multipole interactions and retardation effects are neglected. Consider the truncated spheres to be distributed on the substrate, with a pair correlation function, $g_w(r)$. Taking local field effects into account [22] we can calculate the surface polarizabilities from

$$\gamma = \frac{\langle \alpha_\parallel^s \rangle}{1 - \frac{1}{3}(\varepsilon_a t_\parallel^{opt})^{-1}\langle \alpha_\parallel^s \rangle} \tag{3}$$

$$\beta = \frac{\langle \alpha_\perp^s \rangle}{1 + \frac{1}{3}(\varepsilon_a t_\perp^{opt})^{-1}\langle \alpha_\perp^s \rangle}. \tag{4}$$

Here $\langle \alpha_\parallel^s \rangle$ and $\langle \alpha_\perp^s \rangle$ are the average polarizabilities of the particles per unit surface area, in the directions parallel and normal to the surface of the substrate and ε_a is the dielectric function of the ambient. The corresponding optical thicknesses, $t_\parallel^{opt}$ and $t_\perp^{opt}$ are defined as

$$t_\parallel^{opt} = \frac{4}{3\varepsilon_a}\left[\int_0^\infty \frac{\mathrm{d}r}{r^2}\, g_w(r)\left\{1 + \frac{\varepsilon_a - \varepsilon_s}{\varepsilon_a + \varepsilon_s}\frac{r^3(r^2 - 8d^2)}{(r^2 + 4d^2)^{5/2}}\right\}\right]^{-1} \tag{5}$$

$$t_\perp^{opt} = \frac{4}{3\varepsilon_a}\left[\int_0^\infty \frac{\mathrm{d}r}{r^2}\, g_w(r)\left\{1 - \frac{\varepsilon_a - \varepsilon_s}{\varepsilon_a + \varepsilon_s}\frac{r^3(r^2 - 8d^2)}{(r^2 + 4d^2)^{5/2}}\right\}\right]^{-1}. \tag{6}$$

The first term in the parentheses represents the interactions of a particle with the direct static dipole fields of the other particles, whereas the second term represents the interactions with the images of these dipoles. A physically realistic model of surface roughness must take into account the distribution of feature shapes seen in figure 1(b). As a first approximation to a surface with a broad shape distribution, we calculated $\alpha^s_{\parallel,\perp}$ for truncated spheres and holes, with ten different truncation parameters between -0.9 and 0.0. We then took each particle to be specified by an average polarizability $\langle\alpha^s_{\parallel,\perp}\rangle$ and an average distance from the substrate surface, $\langle d\rangle$. In the case with both bumps and pits present on the surface the average polarizabilities were given by

$$\langle\alpha^s_{\parallel,\perp}\rangle = \eta\langle\alpha^s_{\parallel,\perp}\rangle_{bumps} + (1-\eta)\langle\alpha^s_{\parallel,\perp}\rangle_{pits} \tag{7}$$

where η is the volume fraction of bumps compared to the total volume of inhomogeneities.

The pair correlation function specifies the distribution of particles with an average polarizability and average distance to the substrate surface. In our calculations we took the bump (pit) height (depth) and the surface coverage to be constant. The function $g_w(r)$ was then approximated by

$$g_w(r) = \begin{cases} 0 & r < r_{min} \\ \dfrac{r - r_{min}}{r_{max} - r_{min}} & r_{min} < r < r_{max} \\ 1 & r > r_{max} \end{cases} \tag{8}$$

where r_{min} and r_{max} were obtained from the assumed feature height and surface coverage.

From the surface polarizabilities we subsequently obtain the following amplitude reflection coefficients for the s- and p-polarized electromagnetic field [21]:

$$r_s = \frac{n_a\cos\theta - n_s\cos\theta_t + \mathrm{i}(\omega/c)\gamma}{n_a\cos\theta + n_s\cos\theta_t - \mathrm{i}(\omega/c)\gamma} \tag{9}$$

$$\begin{aligned} r_p = \{&(n_s\cos\theta - n_a\cos\theta_t)[1 - (\omega/2c)^2\varepsilon\gamma\beta\sin^2\theta] - \mathrm{i}(\omega/c)\gamma\cos\theta\cos\theta_t \\ &+\mathrm{i}(\omega/c)n_a n_s\varepsilon\beta\sin^2\theta\}\{(n_s\cos\theta + n_a\cos\theta_t)[1 - (\omega/2c)^2\varepsilon\gamma\beta\sin^2\theta] \\ &-\mathrm{i}(\omega/c)\gamma\cos\theta\cos\theta_t - \mathrm{i}(\omega/c)n_a n_s\varepsilon\beta\sin^2\theta\}^{-1} \end{aligned} \tag{10}$$

where n_s and n_a are the complex indices of refraction for the substrate and the ambient, respectively, θ is the angle of incidence and θ_t is the angle of transmittance.

We now discuss the accuracy of the dipole approximation for the interactions between the truncated spheres. Haarmans and Bedeaux [21] showed that for gold spheres on sapphire the dipole approximation works well for a coverage of up to 50%. The situation we consider is a little different, though. In the reststrahlen band, ionic materials have dielectric functions of 'metallic' character. It is seen in equations (5) and (6) that the term representing the interaction of a particle with the image dipoles of the other particles diverges for $\varepsilon_s = -\varepsilon_a$. For ionic compounds this occurs between ω_L and ω_T, i.e. in the region of the reststrahlen band. Taking into account a physically realistic small imaginary part of ε_s, it is seen from equation (3) and (4) that the surface polarizabilities become mainly imaginary and the reflectances in equation (9) and (10) can take unphysical values larger than the reflectance of the substrate and even larger than unity. Hence the dipole approximation is deficient for frequencies where ε_s is close to $-\varepsilon_a$, and is useful only for low coverages. This limitation prevents us from making more than qualitative comparisons of the bump model with experiments.

4. Results

4.1. Comparison of the EMA to measurements

In the Bruggeman EMA the effective dielectric function, $\langle\varepsilon\rangle$, depends on the filling factor, f and on the depolarization factors L_m and L_p. The density of the polycrystalline beryllia sample is 96% of the density of single crystalline beryllia, i.e. the filling factor of voids, $f = 0.04$, if we assume the sample to be homogeneous and isotropic. We varied the depolarization factor L_p between 0 and 0.5 in order to fit the measured reflectance curves. The parameter L_m does not affect the calculation much because the filling factor is so high. The best fit was obtained for $L_p = 0.5$, which means that we consider the voids to be randomly oriented cylinders. For $L_p = 0.5$ the imaginary part of the effective dielectric function, $\langle\varepsilon_2\rangle$, attains a broad maximum at about 10 μm, superimposed on the Lorentzian behaviour. This maximum corresponds to a minimum in the reflectance.

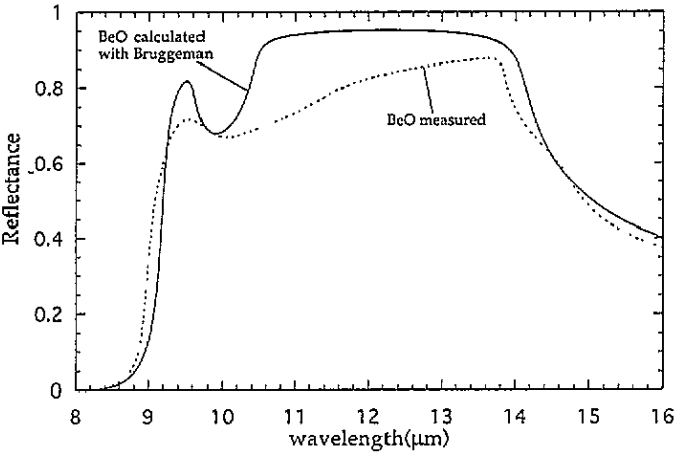

Figure 3. Experimental (dashed) and calculated (full line) reflectance for beryllia as described in the text. The calculated spectrum was obtained with a Bruggeman EMA with $L_p = 0.5$ and $L_m = 0.3$.

In figure 3 the measured reflectance is compared with the Bruggeman EMA for normal incidence. The data are in rough qualitative agreement, but the minimum in the calculated reflectance curve falls at too short a wavelength. The minimum in the measured reflectance curve is broader than in the calculated curve and the calculated reflectance is significantly higher. Figures 4(a) and 4(b) show the measured and calculated reflectance at an angle of incidence of 60° for s- and p-polarized light, respectively. The fits are generally better than at normal incidence but again there are disagreements regarding the position and width of the reflectance minimum. It is seen that there occurs a dip in the measured reflectance curve at about 9.1 μm for p-polarized light, which is not detectable in the calculated curve.

To further test if the structure in the reststrahlen band is due to phonon absorption in the cavities we coated the sample with paraffin oil (Nujol) which has a low absorption in the infrared. The oil may penetrate into the pores just under the surface. The calculated and experimental reflectance spectra for Nujol-coated beryllia as well as the reflectance for Nujol on an aluminium substrate are shown in figure 5. In the calculation the absorption of the paraffin oil was neglected and the dielectric function used for the oil was $\varepsilon = n^2 = 2.25$. The calculated spectrum for the coated sample reproduces well the experimental shift of

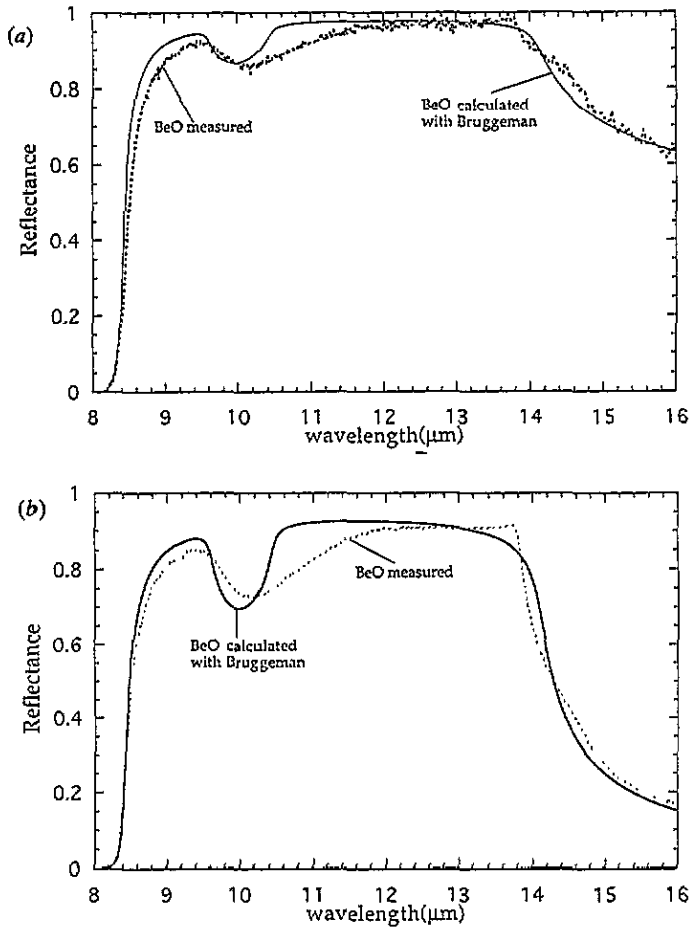

Figure 4. Experimental (dashed) and calculated (full line) reflectance for beryllia, at an angle of incidence of 60°, for (a) s-polarized light and (b) p-polarized light. The calculated spectra were obtained with a Bruggeman EMA with $L_p = 0.5$ and $L_m = 0.3$.

the reflectance dip towards longer wavelengths. The measured values are lower than the calculated ones, because of absorption in the Nujol.

It is seen that the EMA model exhibits qualitative agreement with our experiments. Obtaining improved agreement is possible by using a general distribution of depolarization factors, but we are not convinced of the applicability of such a model to our experimental situation. Because of the lack of detailed agreement, between theory and experiment, we think that the pores in the substrate are not the sole reason for the structure in the reststrahlen band.

4.2. Comparison of the bump model to measurements

Figure 1 shows an SEM and an AFM picture of the polycrystalline beryllia sample and from this picture it is obvious that the surface is covered with different kinds of inhomogeneities. The bump model cannot be used for high surface densities of the particles, which is a considerable restriction. The model is specially sensitive to high coverages close to

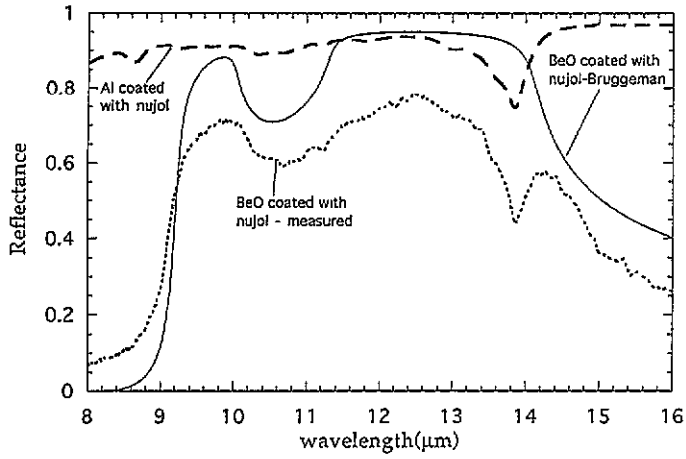

Figure 5. Calculated spectrum (full curve), using the Bruggeman EMA, compared with the corresponding experimental spectrum (dotted curve) for beryllia coated with Nujol. The strength and position of the absorption bands in the coating material are illustrated by the third curve (dashed).

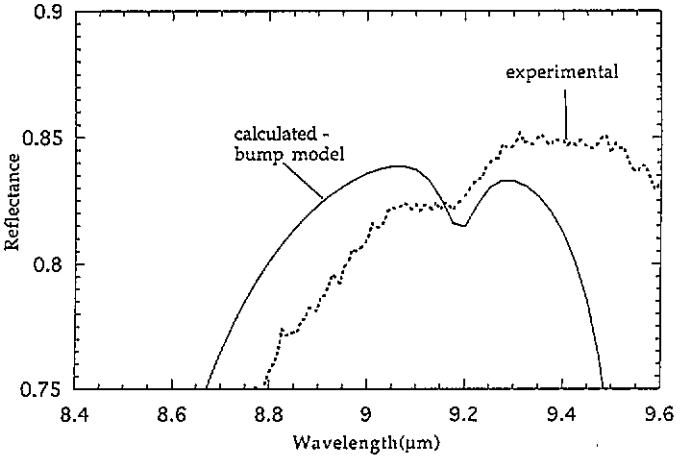

Figure 6. Experimental (dotted curve) and calculated (full curve) reflectance, at an angle of incidence of 60°, for p-polarized light in the region close to the longitudinal optical mode. In the calculation, the height of the particle is 1 μm and the particle density is 50%. The dip at 9.15 μm occurs because the longitudinal optical phonon is excited in inhomogeneities at the surface.

the wavelength where $\varepsilon = -\varepsilon_a$, which occurs for uncoated beryllia at a wavelength of 9.93 μm. In our calculations we therefore use a very low particle coverage, and study only the qualitative features of the spectra. In order to obtain a more accurate result the particle–particle interaction must be expanded to higher multipolar orders.

The most detailed comparison between experiment and theory was carried out in the wavelength region 8.5–9.5 mm. Here the interaction between the particles and the image dipoles is weak and we may assume that the bump model works well for a coverage of up to 50%, which was previously shown to be the case for gold particles on sapphire [21]. We

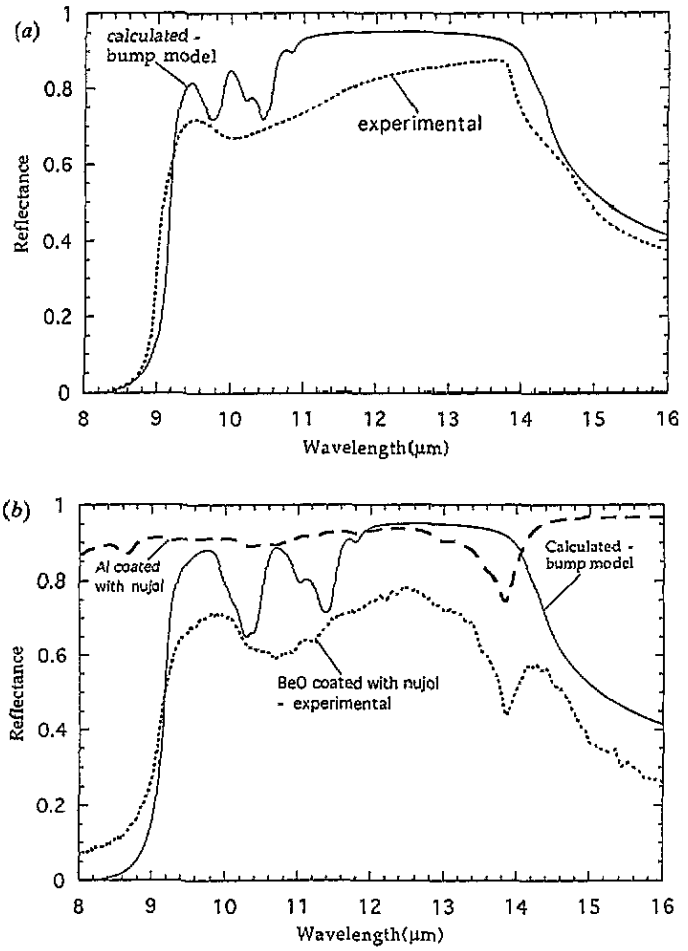

Figure 7. (a) Experimental (dotted) and bump-model-calculated (full line) reflectance for beryllia. (b) Experimental (dotted) and bump-model-calculated (full line) reflectance for Nujol-coated beryllia. The strength and position of the absorption bands in the coating material is illustrated by the third curve (dashed).

consider the particles to be distributed randomly with a certain pair correlation function. The coverage was taken to be 50%, which is much less than inferred from figure 1(a) and (b). In order to partially compensate for this, the height of the particles was taken to be 1 μm, which is higher than in the AFM picture. Most of the inhomogeneities were taken to be bumps, $\eta = 0.9$ in equation (7), which seems to be a reasonable assumption according to the SEM picture in figure 1(a). These parameters lead to a correlation function specified by $r_{min} = 3$ μm and $r_{max} = 11$ μm, whereas $\langle d \rangle$ was found to be 1.93 μm. In figure 6 the calculated reflectance for p-polarized light at 60° is shown. The calculated and measured spectra show, at the same wavelength, a small dip in the reflectance. This dip occurs where the value $\mathrm{Im}(-1/\varepsilon)$ is a maximum, i.e. the longitudinal optical phonon is excited in our samples. A dip at this wavelength cannot be understood on the basis of the EMA. However, we have shown before [9] that the LO mode can be excited by p-polarized light at oblique angles of incidence, if the substrate surface is partly covered by small truncated spheres.

The experimental observation of this feature constitutes an unambiguous proof that bumps on the surface significantly influence the shape of the reststrahlen band in beryllia.

Finally we present a qualitative comparison of the theory and experiment over the whole wavelength range. Because of the problems with the bump model mentioned above, the coverage was only taken to be 10%. The height (depth) of the particles are again taken to be 1 μm and η to be 0.9, which leads to $r_{min} = 5$ μm and $r_{max} = 30$ μm. In figure 7(a) the measured and calculated reflectance are compared. The calculation exhibits several reflectance minima, but their positions approximately correspond to the much smoother experimental minimum. At about 10 μm a maximum in the calculated spectrum is seen. This peak is an artifact which occurs when $\varepsilon_s = -\varepsilon_a$, as explained above. It is expected to be smeared out for higher surface densities and more accurate representations of particle–particle interactions. The calculated reflectance from Nujol-coated beryllia is compared in figure 7(b) with the measured one. The minimum shifts in both spectra, but the artificial maximum in the calculated curve (now at 10.6 μm) distorts the shape of the calculated spectrum.

5. Conclusions

We have demonstrated, experimentally and theoretically, that phonon absorption in cavities in the bulk and in inhomogeneities at the surface can modify the features of the infrared reststrahlen band. In this study we specifically considered BeO, but these absorption effects are general for all ionic materials.

In our theoretical study we have used the Bruggeman EMA, in order to take the phonon absorption in the voids into account, and the so-called 'bump model' to describe phonon absorption in the structures at the rough surface. Both models give spectra with reflectance minima in the reststrahlen band, in qualitative agreement with experiments. When the samples were coated with paraffin oil, we noticed a wavelength shift of the minimum in the reststrahlen band in agreement with both models. Probably phonon absorption in both the cavities in the bulk and inhomogeneities on the surface gives significant contributions to the measured spectra.

A clear indication of the importance of bumps at the surface was provided by measurements of p-polarized reflectance at an angle of incidence of 60°. We observed that the longitudinal optical mode was excited. This is possible for a bulk sample only in bumps at the surface [9].

Acknowledgements

We are grateful to Dr P Bobbert, University of Eindhoven, for providing us with a computer program for solving Laplace's equation and we appreciate illuminating discussions with Dr C G Ribbing. We are also grateful to Filip Bergman and Rickard Gåhlin who helped us with the AFM pictures, and Dr Mikael Olsson is acknowledged for carrying out the SEM study. Financial support for this work was provided by The Swedish Natural Science Research Council and The National Defence Research Establishment.

References

[1] Ruppin R and Engelman R 1970 *Rep. Prog. Phys.* **33** 149
[2] Fröhlich H 1949 *Theory of Dielectrics* (London: Oxford University Press)
[3] Bohren C F and Huffman D R 1983 *Absorption and Scattering of Light by Small Particles* (New York: Wiley)

[4] Barker J A S 1963 *Phys. Rev.* **132** 1474
[5] Berreman D W 1967 *Phys. Rev.* **163** 855
[6] Wind M M, Vlieger J and Bedeaux D 1987 *Physica* A **141** 33
[7] Wind M M, Bobbert P A, Vlieger J and Bedeaux D 1987 *Physica* A **143** 164
[8] Bobbert P A and Vlieger J 1987 *Physica* A **147** 115
[9] Andersson S K and Niklasson G A 1995 *J. Phys.: Condens. Matter* **7** 7173
[10] Chibuye T, Ribbing C G and Wäckelgård E 1994 *Appl. Opt.* **33** 5975
[11] Loh E 1968 *Phys. Rev.* **166** 673
[12] Andersson S K and Ribbing C G 1994 *Phys. Rev.* B **49** 11336
[13] Bruggeman D A G 1935 *Ann. Phys., Lpz.* **24** 636
[14] Berreman D W 1963 *Phys. Rev.* **130** 2193
[15] Yen Y-S and Wong J S 1989 *J. Phys. Chem. Solids* **93** 7208
[16] Yamamoto K and Ishida H 1994 *Vib. Spectrosc.* **8** 1
[17] Lyddane R H, Sachs R G and Teller E 1941 *Phys. Rev.* **59** 673
[18] Bohren C F and Gilra D P 1979 *J. Colloid. Interface Sci.* **72** 215
[19] Pecharromán C and Iglesias J E 1994 *J. Phys.: Condens. Matter* **6** 7125
[20] Born M and Wolf E 1980 *Principles of Optics* (Oxford: Pergamon)
[21] Haarmans M T and Bedeaux D 1993 *Thin Solid Films* **224** 117
[22] Vlieger J and Bedeaux D 1980 *Thin Solid Films* **69** 107